VISTA Status Report
December 1993

S. Halama, C. Pichler, G. Rieger, S. Selberherr, T. Simlinger, H. Stippel, E. Strasser

Institute for Microelectronics
Technical University Vienna
Gusshausstrasse 27-29
A-1040 Vienna, Austria

Contents

Summary

The last six months have brought strong efforts to further improve the VISTA system. While the most important tools of the framework have been improved, the integration of the simulators of the Institute for Microelectronics has been carried on.

A new tool provides triangulation and gridding facilities for arbitrary geometries. It is implemented using a combination of some very efficient algorithms.

A new module for simulation of etching and deposition has been developed from scratch with respect to the VISTA integration in an early constructing phase. It is capable of simulating a variety of topography processes on arbitrary structures.

The analytic and Monte Carlo ion implantation parts of the PROMIS process simulator have been finished and coupled to the VISTA framework on data and task level.

The two dimensional VISTA visualization package has been considerably improved to satisfy even pretentious needs.

Based on the experience gained from the first implementation of the Simulation Flow Control Module (SFC), a graphical simulation flow editor (SFED) has been developed that allows the definition of simulation flow sequences in terms of tool calls.

1 The VORONOI Gridding Service

1.1 Aims

The program system VORONOI is part of the VISTA framework and provides general purpose two-dimensional triangular grid generation services. VORONOI is currently implemented as a monolithic stand-alone application which reads and writes PIF data.

Currently, the major aim of the gridding tool VORONOI is to provide *robust* and *fast* two-dimensional geometry-conformal triangulation of raw grid data. In other words, given any non-planar complex PIF geometry and any set of "raw" grid points (which need not coincide with the geometry in any form), VORONOI creates a triangular Delaunay grid which consists of the input grid points and additional points on the boundary of the input geometry.

This is very valuable for creating mutually consistent grid and geometry representations after simulation steps that affect either the geometry or the grid, but not both. This is usually the case for the simulation of etching and deposition (geometry only, "don't care about attributes and grids") or for solely orthoproduct-based simulators (like the PROMIS Monte Carlo module for ion implantation), which do not (and can not) care about geometry conformity of the grid.

1.2 Architecture

VORONOI consists of several modules which operate on the grid data, or more precisely, the Delaunay and Voronoi graph. The simplified algorithm for the triangulation is:

1 Read PIF geometry. This defines all initial boundary and interface edges and boundary nodes.

2 Build a quadtree and store all geometrical nodes in it.

3 Read all PIF grid points and add them as initial grid nodes into the quadtree (without connecting them).

4 Refine existing boundaries to guarantee geometry conformity of the future Delaunay triangulation.

5 Remove all (boundary and interface) edges.

6 Triangulate all Delaunay nodes.

7 Remove exterior Delaunay edges.

8 Write PIF output grids.

Additional steps can (and will) be added between the existing 8 steps, increasing the abilities of the VORONOI gridder. These include, for instance, the addition and removal of inner grid-points according to a grid density control function, the relaxation of grid point positions, or the decomposition of complex geometries into triangular faces.

Special attention has been paid to choose optimal or near-optimal algorithms for the steps 2, 4, 5, 6, and 7.

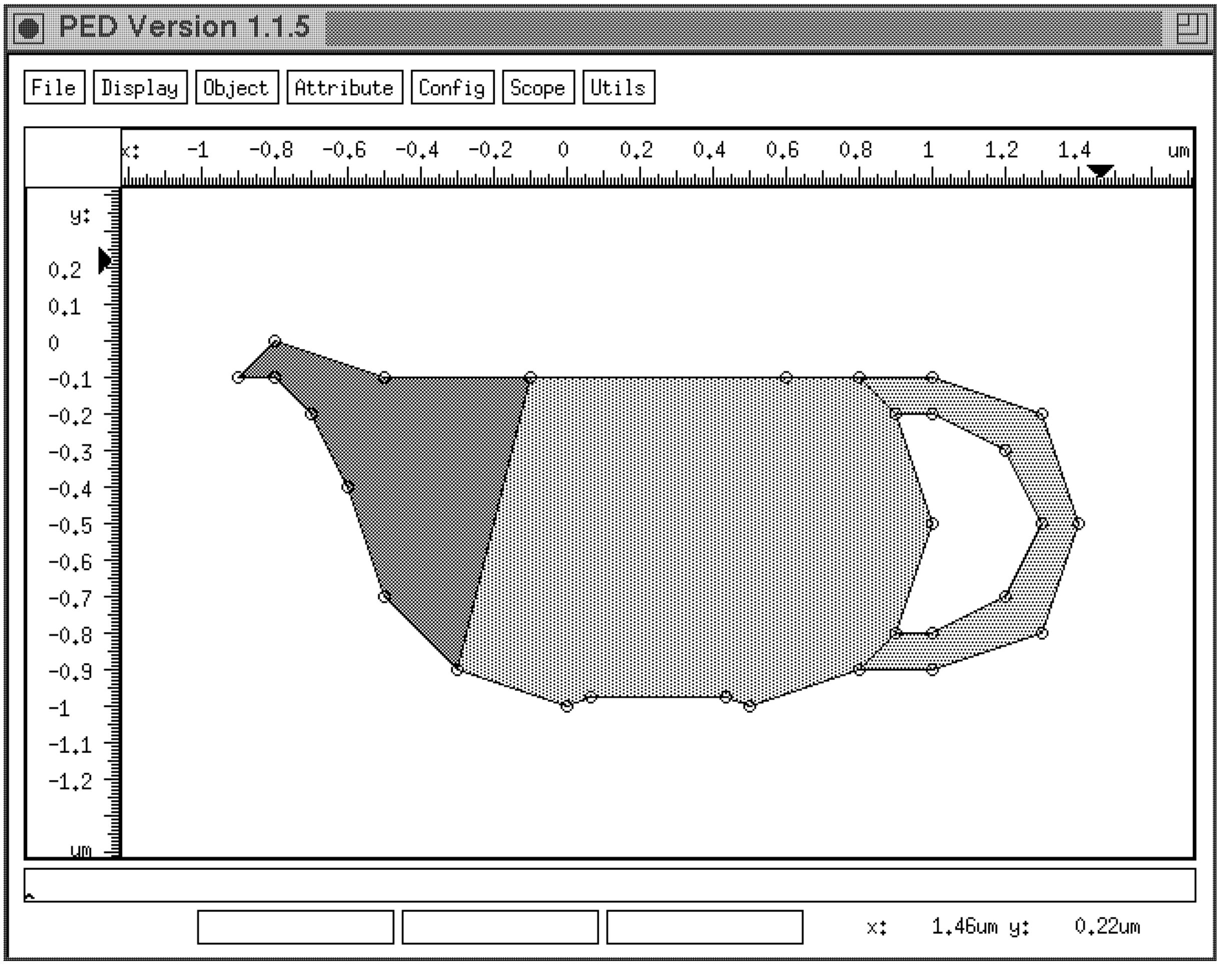

Figure 1: The Initial PIF Geometry

Given an input PIF geometry like in fig. 1 (this very simple PIF input without inner grid points is only used for illustration of the algorithm and data structures), all the input points (this example does not have input grid points) are stored in a quadtree structure (fig. 2) as initial nodes of the Delaunay graph.

In the subsequent boundary refinement step, a loop over all boundary edges is performed and for every edge, a set of points is selected. These points are "suspected triangulation candidates" — they might form a triangle with the boundary edge under consideration in the subsequent triangulation step. If the angle adjacent to the boundary edge would then be obtuse, the edge needs to be refined. This is done by adding a new Delaunay node at a certain position on the edge.

All these boundary edges are then removed as they would interfere with the subsequent triangulation process. All removed edges will later be reproduced by the triangulation (it is the actual task of the refinement step to guarantee that).

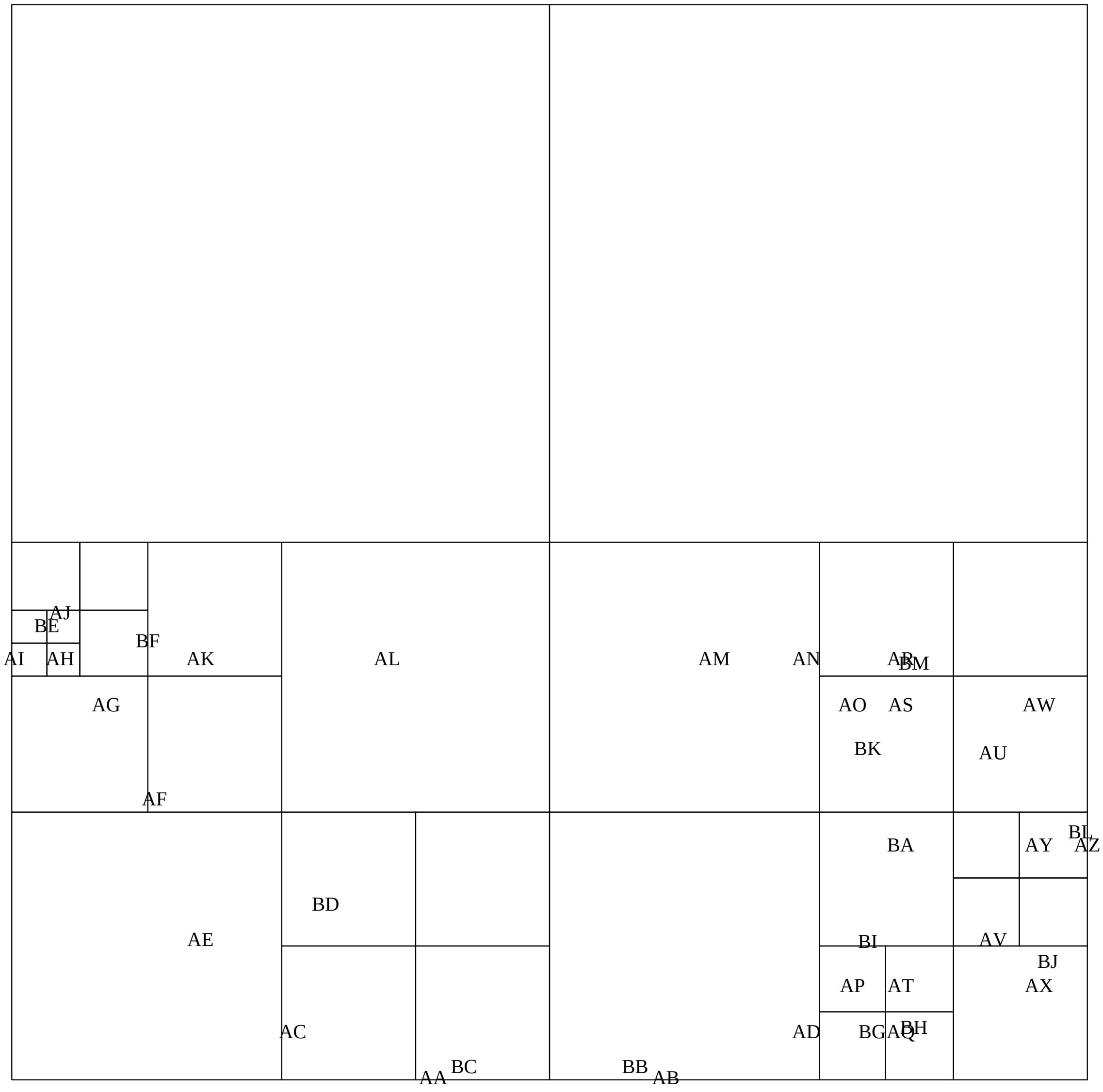

Figure 2: Quadtree used to store and locate the Delaunay grid points (already after boundary refinement).

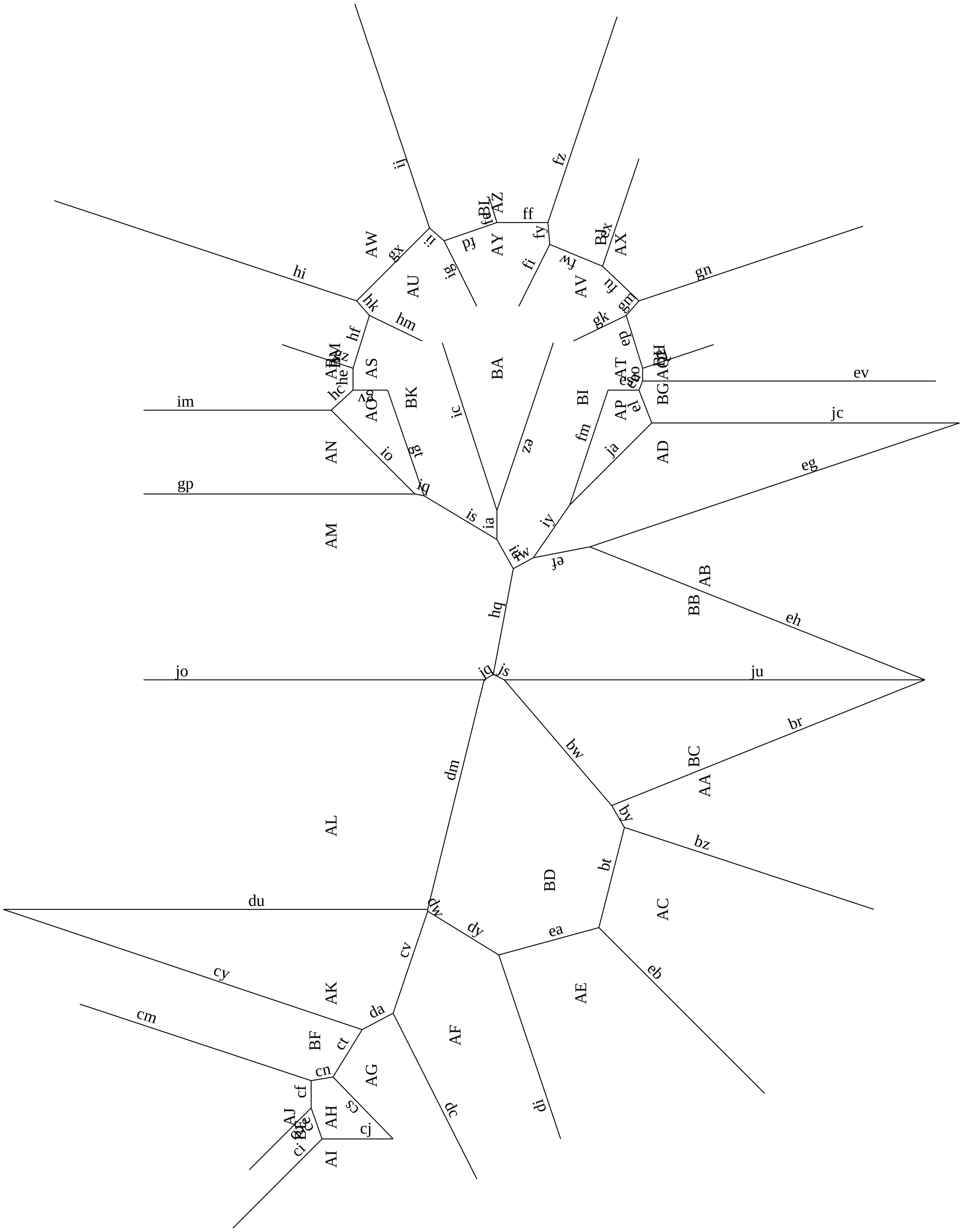

Figure 3: Voronoi Graph after Exterior Edge Removal

Then a Voronoi tessellation is performed which yields the Voronoi graph (fig. 3) and its dual graph, the Delaunay triangulation (fig. 4).

As can be seen in fig. 4, all geometrical edges which have been in the input PIF are properly reproduced in the resulting grid.

1.3 Implementation Aspects

1.3.1 Data Structures

The initial data structures and algorithms for the triangulation have been taken from Preparata and Shamos [1], pp. 215–219. It should be noted that this algorithm is mainly of theoretical value, as it excludes many important practical applications by assuming 1) that not more than 3 point lie on a circle, 2) that point subsets are not collinear, 3) that Delaunay edges are not parallel, and 4) by not accounting for finite precision arithmetics.

This is why considerable extensions and modifications to the original algorithm and data structures had to be made. Many important input grids are tensor-product based and hence the special cases of collinear and cocircular points are very likely to occur. The most severe modification, however, is the use of a *point bucket quadtree*[2] for the storage of grid and geometry points.

There is no distinction in the basic data structures used to represent the Delaunay and Voronoi graph. Unified atomic data structures are used for storing the Delaunay nodes and edges and the Voronoi nodes and edges. *Doubly Connected Edge Lists* (DCELs) are used for both the Delaunay and Voronoi Graph.

To store and find the Delaunay nodes, a *point bucket quadtree* is used. The recursive data structure consists of a *quadtree root*, *quadtree branch buckets* (containing four sub-buckets which can either be branch buckets or leaf buckets) and *quadtree leaf buckets*. The leaf buckets contain a maximum of three *Delaunay nodes* (see also fig. 2).

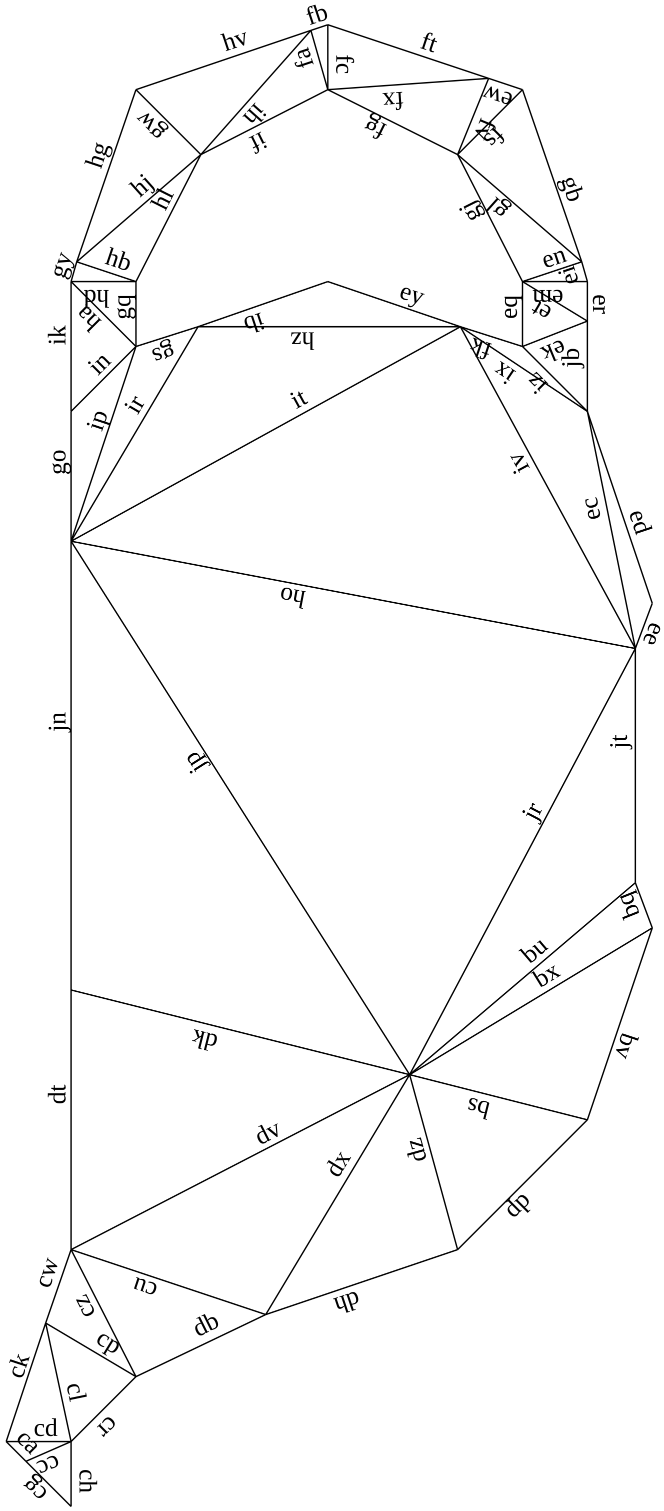

Figure 4: Delaunay Graph after Exterior Edge Removal

1.3.2 Performance

The theoretically predicted *average* computational complexity for the boundary refinement is $M \cdot log(N)$ and for the actual triangulation it is $N \cdot log(N)$ (where M is the number of boundary edges after refinement and N is the number of Delaunay nodes).

Fig. 5 shows the measured performance[1] of the most important algorithms. Realistic input data with a variety of geometries and input grid point clouds have been used. CPU time measurements have been performed on a DECstation 5000/200, Ultrix V4.3 native C compiler.

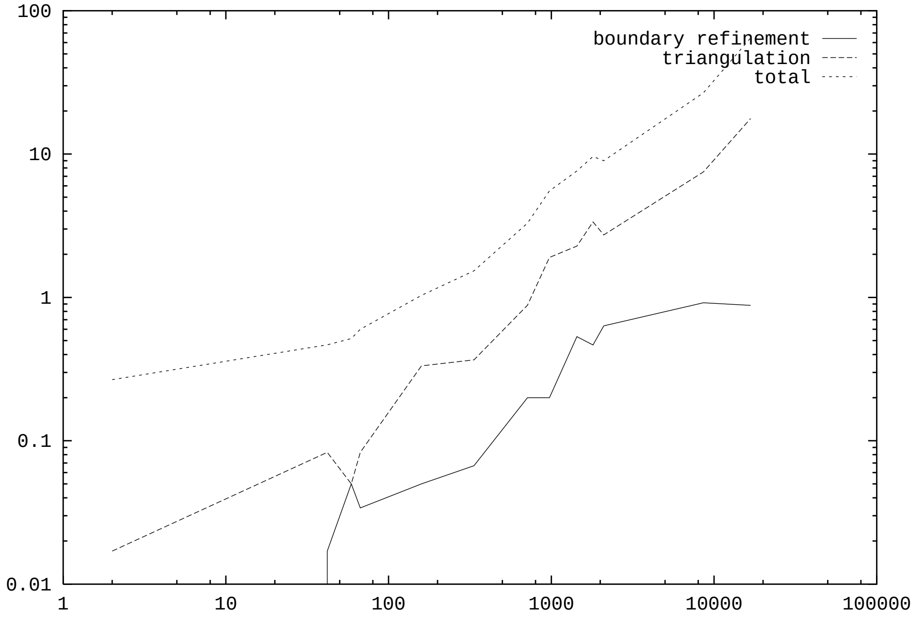

Figure 5: CPU time (in seconds) of the gridding process as a function of the number of triangles generated. Boundary refinement (steps 4 and 5), sole triangulation (step 6) and total CPU time (including PIF I/O).

[1] The evaluation reflects the status of VORONOI as of 1993-12-22

2 The VISTA Etching and Deposition Module

As a part of the VISTA Process Simulation Tools a program for modeling etching and deposition processes has been developed. The program can handle arbitrary geometries containing regions of arbitrary materials. The basic process steps simulated are wet and dry etching, as well as isotropic and unidirectional deposition.

Etching and deposition processes are simulated based on morphological operations derived from image and signal processing [3]. These operations provide a well defined methodology to simulate the time evolution of topographical features during an etching or deposition process [4]. Together with a cellular material representation this method allows an accurate and stable simulation of arbitrary structures.

2.1 Structure

The program gets its initial geometry from a PIF Binary File. The initial geometry can either be a simulation result from a previous simulation run or a geometry constructed with the interactive PIF Editor. The program uses the VISTA Two-dimensional Geometry Support Library to read the input geometry from a PIF Binary file and to perform the point location used for initializing the cellular structure. In addition the program reads several control parameters from the command line and material information such as default etch rates from the VISTA Material Server. After running one of the topography processes a marching square algorithm is applied to obtain surface polygons from the cellular structure. Finally, the VISTA Two-dimensional Support Library is used to store the simulation result again in a PIF Binary File.

2.2 User Interface

A graphical user interface which was built on the VISTA User Interface allows a comfortable usage of the program for all of the topography processes. The panel for anisotropic etching as it appears on screen is shown in fig. 6. All input parameters needed for a simulation run can be set here by the user. Each panel consists of three sections. The first one is titled *Input Geometry* to specify from which PIF file to read the initial geometry and to define the name of the PIF input geometry. The second part is titled *Output Geometry* to specify which PIF file should be used to store the simulation result and to define the name of the PIF output geometry. The last section is titled *Input Parameters* and consists of several input keys which are either physical parameters or simulator specific keys.

The panels for the etching processes in addition have a button which is called *Material Definitions.* When pressed an additional window appears as shown in fig. 7 which allows the change of the default etch rate for a material.

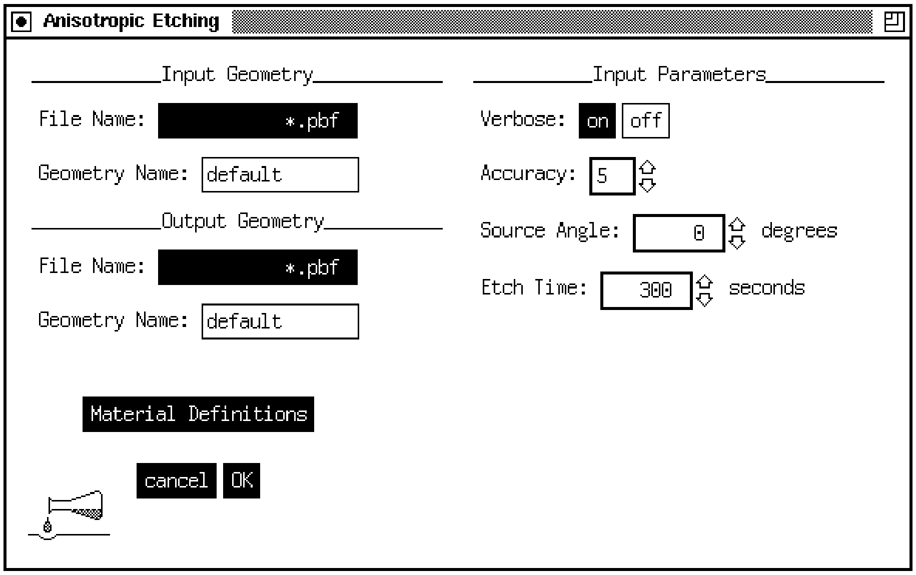

Input Geometry

File Name: *.pbf

Geometry Name: default

Output Geometry

File Name: *.pbf

Geometry Name: default

Input Parameters

Verbose: [✓ on] off

Accuracy: 5

Source Angle: 0 degrees

Etch Time: 300 seconds

Figure 6: Panel for Anisotropic Etching

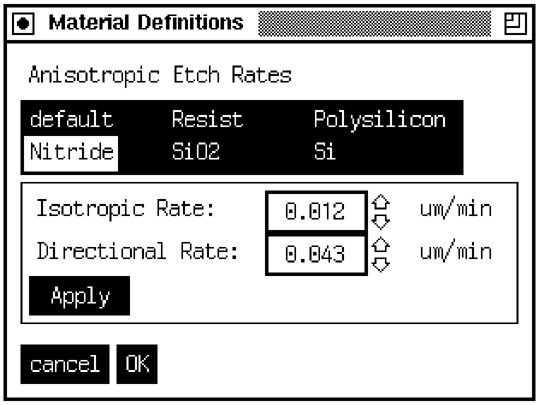

Anisotropic Etch Rates

default	Resist	Polysilicon
[✓ Nitride]	SiO2	Si

Isotropic Rate: 0.012 um/min

Directional Rate: 0.043 um/min

Figure 7: Panel for Specifying the Etch Rates

2.3 Example

This example begins with a planar silicon substrate, a thin oxide layer, and a nitride mask on top. First, an isotropic etching step is performed. The etch rates for the materials are: silicon = 0.03 $\mu m/min$, oxide = 0.006 $\mu m/min$, and nitride = 0.012 $\mu m/min$. The simulation time for the isotropic etching step is 800 seconds. Subsequently, a unidirectional metalization step under 20 degree is performed. The deposition rate is 0.03 $\mu m/min$, the deposition time is 250 seconds. The simulation result after these two process steps is shown in fig. 8.

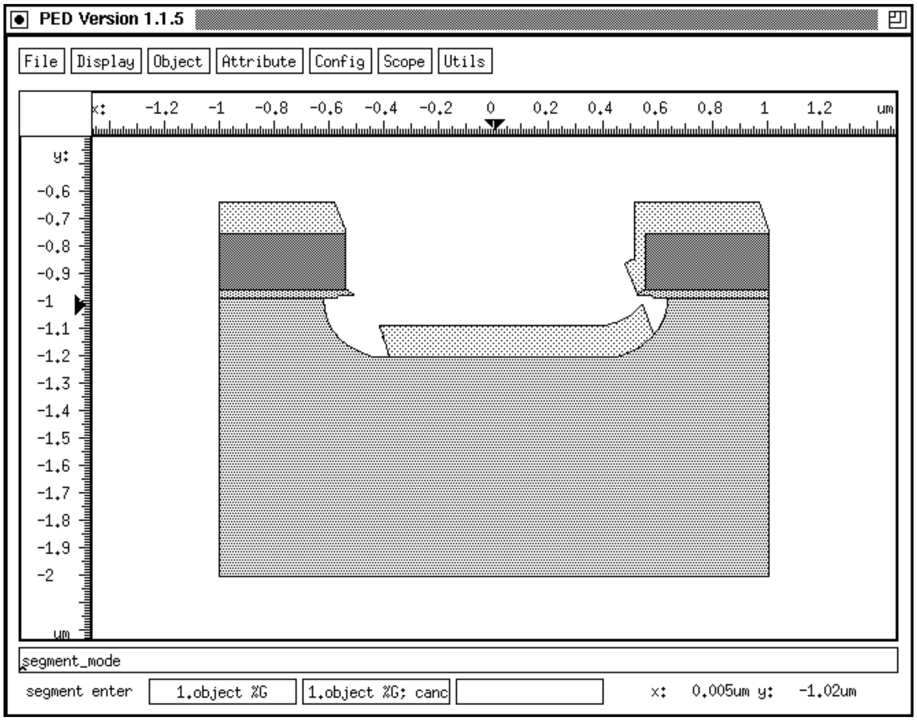
PED Version 1.1.5
File
Display
Object
Attribute
Config
Scope
Utils
x: -1.2 -1 -0.8 -0.6 -0.4 -0.2 0 0.2 0.4 0.6 0.8 1 1.2 um
y: -0.6 -0.7 -0.8 -0.9 -1 -1.1 -1.2 -1.3 -1.4 -1.5 -1.6 -1.7 -1.8 -1.9 -2 um

```
segment_mode
segment enter   1.object %G   1.object %G; canc        x:  0.005um y:  -1.02um
```

Figure 8: Simulation Result after Unidirectional Metalization under 20 Degree

3 PROMIS Ion Implantation in VISTA

Currently the most important technique to induce dopants into the substrate is ion implantation. Consequently, in VISTA this key step for fabrication of modern semiconductor devices can be modeled by two modules derived from the process simulator PROMIS [5, 6]: An analytic [6, 7] and a Monte Carlo ion implantation simulator [8]. Both programs give accurate and reliable results, and beyond that, they are very fast.

3.1 Analytical Modeling of Ion Implantation in VISTA

For the analytical simulation of the ion implantation in VISTA a very general module based on the *numerical range scaling* developed by Ryssel et al. in 1986 [9] with the extensions proposed by Wierzbicki in Wierzbicki et al. [10] is used. For the numerical range scaling the target geometry is subdivided into several stripes. For every stripe the related distribution function is determined describing the point response for the given ion-target material combination. To get the concentration in a certain point the influence from the neighbouring point responses is considered by integrating laterally over the distribution functions. The extension of Wierzbicki is mainly the modification of the lateral range strangling by taking the material layers above the actual layer into account. In addition to this model two-dimensional models as well as one-dimensional distribution functions are available. Finally, the user can specify his/her own, for the company's process especially tailored models.

The module for the analytic simulation of the ion implantation in PROMIS supports the modeling of arbitrary multilayer structures with any implantation angle and a variety of ion-target material combinations. Beyond that, damage generation can be computed, too. The only still existing limitations for the target structure are, that a vacuum region must be explicitly defined and the geometry must be oriented counter-clockwise. But these restrictions will be eliminated soon, although they do not really restrain the simulation of a whole process, because of the already existing geometry simplification routines provided by VISTA.

A short overview of the available models and the possible ion-target material combinations is given in Tables 1 – 3 and the user interface for the invocation of the analytical ion implantation is shown in fig. 9.

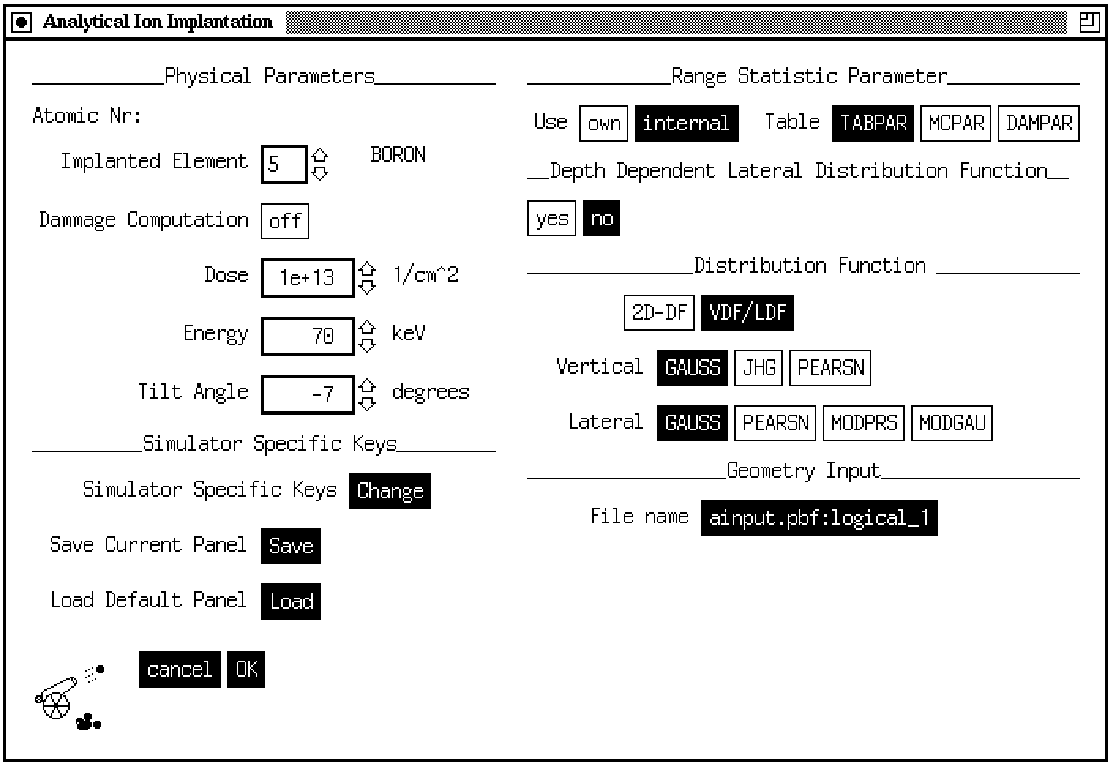

Analytical Ion Implantation

Physical Parameters

Atomic Nr:

Implanted Element 5 BORON

Dammage Computation off

Dose 1e+13 1/cm^2

Energy 70 keV

Tilt Angle -7 degrees

Simulator Specific Keys

Simulator Specific Keys Change

Save Current Panel Save

Load Default Panel Load

cancel OK

Range Statistic Parameter

Use own [✓ internal] Table [✓ TABPAR] MCPAR DAMPAR

Depth Dependent Lateral Distribution Function

yes [✓ no]

Distribution Function

2D-DF [✓ VDF/LDF]

Vertical [✓ GAUSS] JHG PEARSN

Lateral [✓ GAUSS] PEARSN MODPRS MODGAU

Geometry Input

File name ainput.pbf:logical_1

Figure 9: User interface for the invocation of the analytical ion implantation module of PROMIS.

Model	Distribution function	Remark
Gauss	Gaussian	
Jhg	Joined Half Gaussian	
Pearsn	Pearson family	selects the applicable type of Gaussian or Pearson I – Pearson VII depending on skewness γ and kurtosis β
Modgau	Modified Gaussian	*lateral distribution,* $Rp = \gamma = 0$, modified Gaussian distribution function according to Hobler [7]
Pears7	Pearson VII, Modified Gaussian	*lateral distribution,* $Rp = \gamma = 0$, selects Pearson VII or modified Gaussian depending on kurtosis β
Damfun	Gaussian with exponential tail	*vertical damage distribution,* Gaussian distribution function with an exponential tail according to Hobler [7]

Table 1: Distribution functions for the analytical ion implantation module in PROMIS.

Model	Elements	Targets	Remark
Mcmom	B, P, As, Sb	Si, SiO_2, Si_3N_4, $GaAs$	depth dependent lateral moments according to Hoblers Monte Carlo simulations [7]
Dammom	B, P, As, Sb	Si	damage (interstitial, vacancy) profiles in silicon, depth dependent lateral moments according to Hoblers Monte Carlo simulations [7]

Table 2: Depth dependent lateral moment models for the analytical ion implantation module in PROMIS.

Model	Elements	Targets	Remark
Tabpar	B, P, As, Sb, BF_2	Si, SiO_2, Si_3N_4, Poly-Si, Al	tabulated moments from LSS-theory taken from Gibbons [11] modified to include some channeling effects for boron based on data by Slaby, et al. [12]
Mcpar	B, P, As, Sb, Si, Be, Mg, O	Si, SiO_2, Si_3N_4, $GaAs$	range statistics according to Hoblers Monte Carlo simulations [7]
Dampar	B, P, As, Sb	Si	damage (interstitial, vacancy) profiles in silicon, range statistics according to Hoblers Monte Carlo simulations [7]

Table 3: Range parameters for the analytical ion implantation module in PROMIS.

3.2 Monte Carlo Simulation of Ion Implantation in VISTA

The Monte Carlo module is much more flexible and reliable than the analytical simulation tool. For instance in [13] it is shown that the analytical model does not predict the doping profile correct for problems with abrupt changes in the geometry. Any ion-target material combination is possible, and recoils can be followed exactly. Moreover, the Monte Carlo method is more physically based.

There are no restrictions concerning the geometry of the simulated structure in the Monte Carlo simulator. The previously existing 31-point limit was eliminated. For the geometric tests to determine the region where an ion resides the slab method is used. By use of this method about the same simulation times can be reached as before. The elimination of the 31-point limit was necessary to allow the simulation of structures which were generated by a topography simulator, realistically.

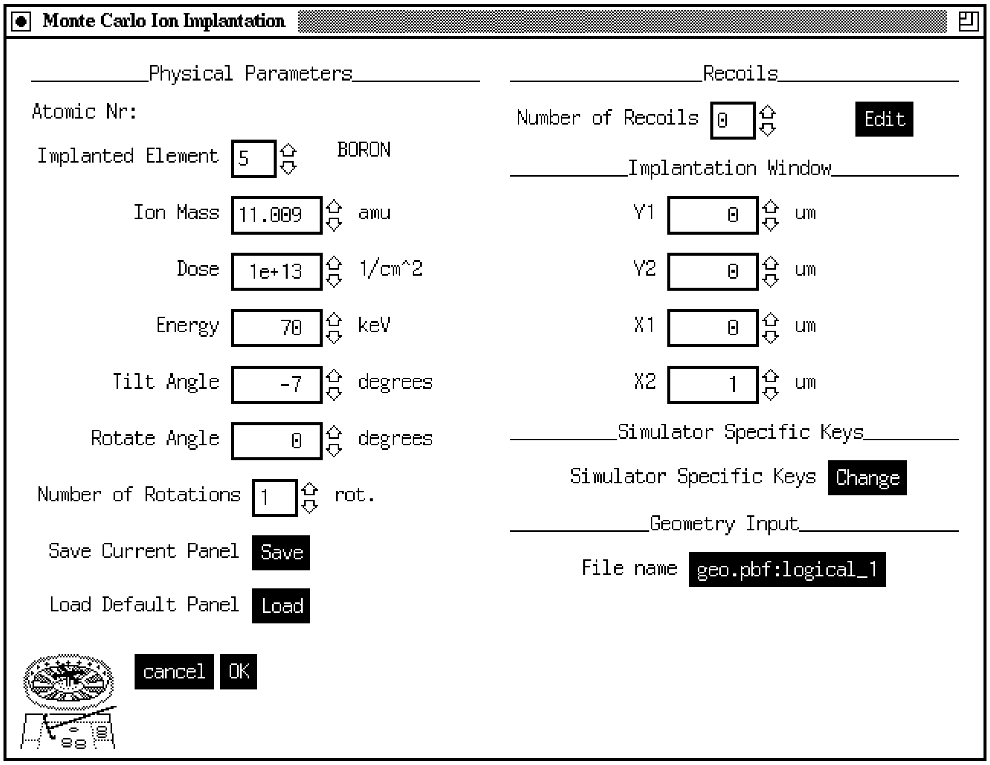

Monte Carlo Ion Implantation

Physical Parameters

Atomic Nr:

Implanted Element 5 BORON

Ion Mass 11.009 amu

Dose 1e+13 1/cm^2

Energy 70 keV

Tilt Angle -7 degrees

Rotate Angle 0 degrees

Number of Rotations 1 rot.

Save Current Panel

Load Default Panel

Recoils

Number of Recoils 0

Implantation Window

Y1 0 um

Y2 0 um

X1 0 um

X2 1 um

Simulator Specific Keys

Simulator Specific Keys

Geometry Input

File name geo.pbf:logical_1

Figure 10: User interface for the invocation of the Monte Carlo ion implantation module of PROMIS.

4 The PIF Visualization

As a result of a simulation process several data will be stored onto a PIF output file. Two dimensional data, which means values of a function of two variables, stored as PIF attributes can be viewed with the PIF visualization tool `xpif2d`.

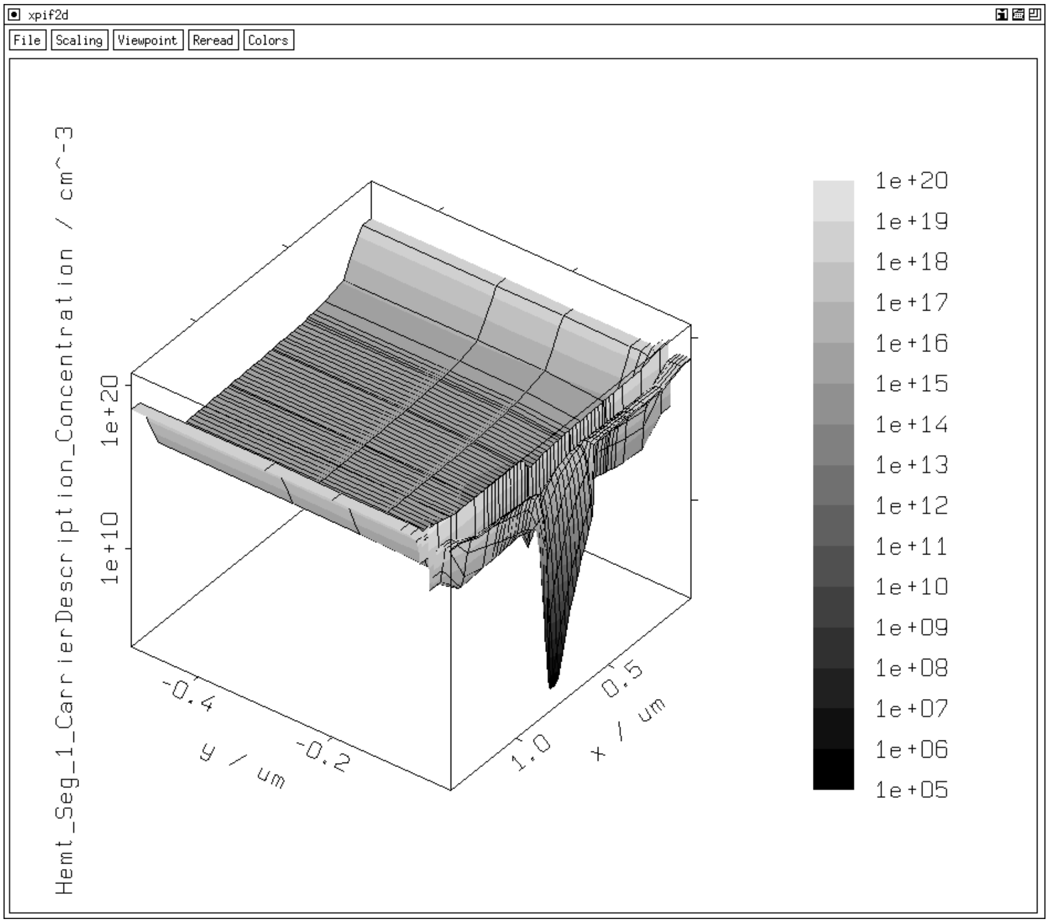

Figure 11: Viewing an electron concentration in logarithmic mode with colored slices and a color scale.

Fig. 11 shows the electron concentration of a transistor device in logarithmic mode with colored slices and a color scale. The data mode features of `xpif2d` include 'logarithmic', 'absolut', 'negative' and 'square' representations and can be arbitrarily mixed. Using the 'square' mode the domain of the independent variables will be scaled so that it is viewed as a square. This is useful if your domain is a small slice.

An arbitrary domain can be selected interactively or by command line resource `-limits 'xmin xmax ymin ymax'`. With a crosshair cursor running in the xy-plane (xy is a placeholder for the 2 independent variables which the attribute to view depends on) the domain can be selected by click and drag. The crosshair axes are parallel to the xy-axes. If a new domain is selected the attribute is cut and displayed using the full display area. So arbitrary details can be viewed.

If the domain is selected by command line, this is the largest selectable domain and the upper bound for all interactively specified subdomains.

Five predefined viewing directions are available. Four from above the attribute with the directions from southeast, southwest, northeast, and northwest and the negative z-direction (top view).

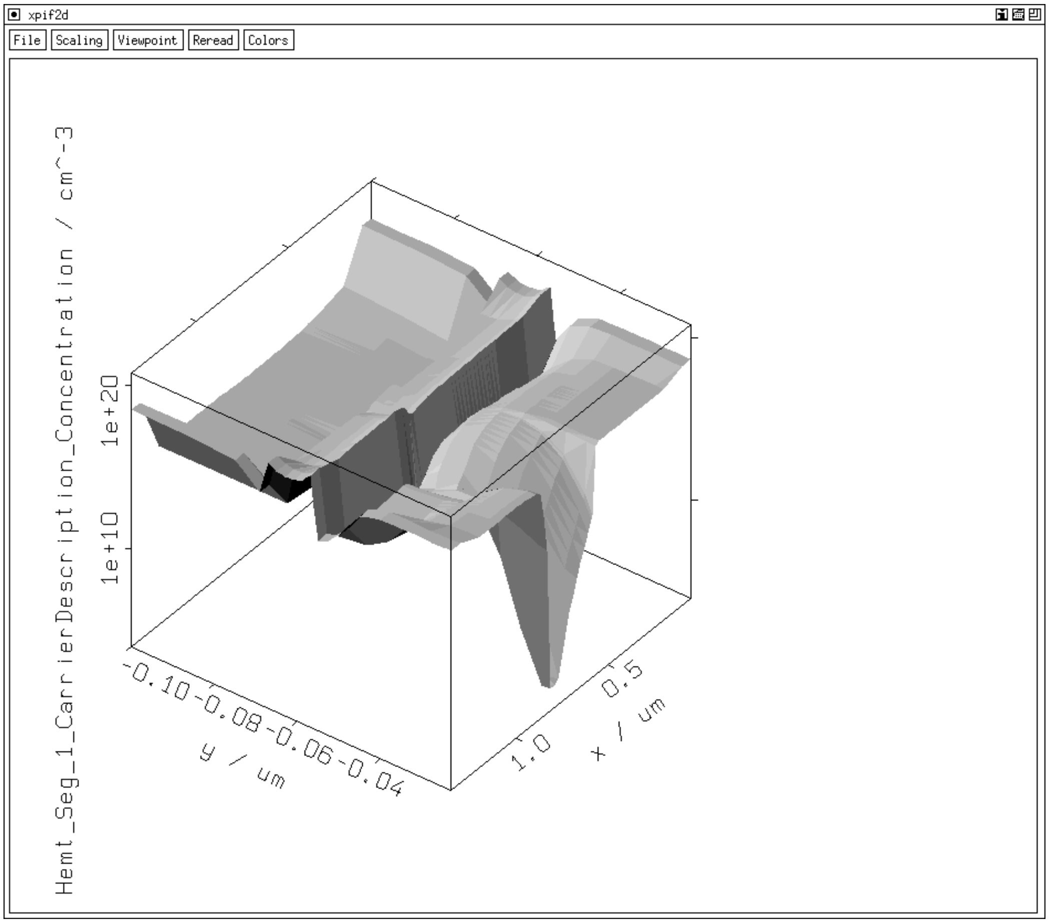

Figure 12: Viewing an electron concentration using the front/back shading color mode.

To obtain an efficient data representation `xpif2d` includes several color modes as ‘color slices’, ‘color isolines’ and ‘front/back shading’. The ‘color slices’ and ‘color isolines’ modes also show a color scale. Fig. 11 is an example with ‘color slices’ mode and a color scale, fig. 12 shows the ‘front/back shading’ mode. For the color scale rainbow colors or the colors of hot iron can be chosen.

The attribute to view must be defined on an ortho product grid or on any grid supported by the ‘unstructured grid support’ of VISTA. Whether the grid is displayed or not is selectable. Is a geometry specified it is displayed as well. Since both, the grid and the geometry, are shown as black lines, especially when the top view is used they are not distinguishable. Therefore, for the geometry a special display mode exists which uses bold lines to emphasize it. Like the crosshair cursor the geometry is drawn in the xy-plane and makes it easier to select a desired subdomain.

5 The VISTA Simulation Flow Control Module

5.1 Work in Progress and Current Concerns

The VISTA Simulation Flow Control Module (SFC) provides a mechanism for defining, editing, and executing multistep semiconductor simulation tasks. In the last six months, the transition from a solely text-based simulation flow description [14] has been made to a graphical flow editor. A number of additional tools have been devised and implemented that complete the set of tools already integrated with respect to the realistic simulation of fabrication process flows, e.g., mask transfer and lithography simulation emulation. The definition of a wafer state description has been tackled to standardize the interaction between independently developed simulators, although no final agreement has been reached yet.

5.2 The Simulation Flow Editor

Based on the VISTA X Library, a block-oriented graphical editor has been built that provides all functionality to define hierarchically structured flow descriptions (ref. fig. 13). Special care has been taken to reuse all existing panels in order to present the user with a uniform interface for tool invocation as well as for flow definition.

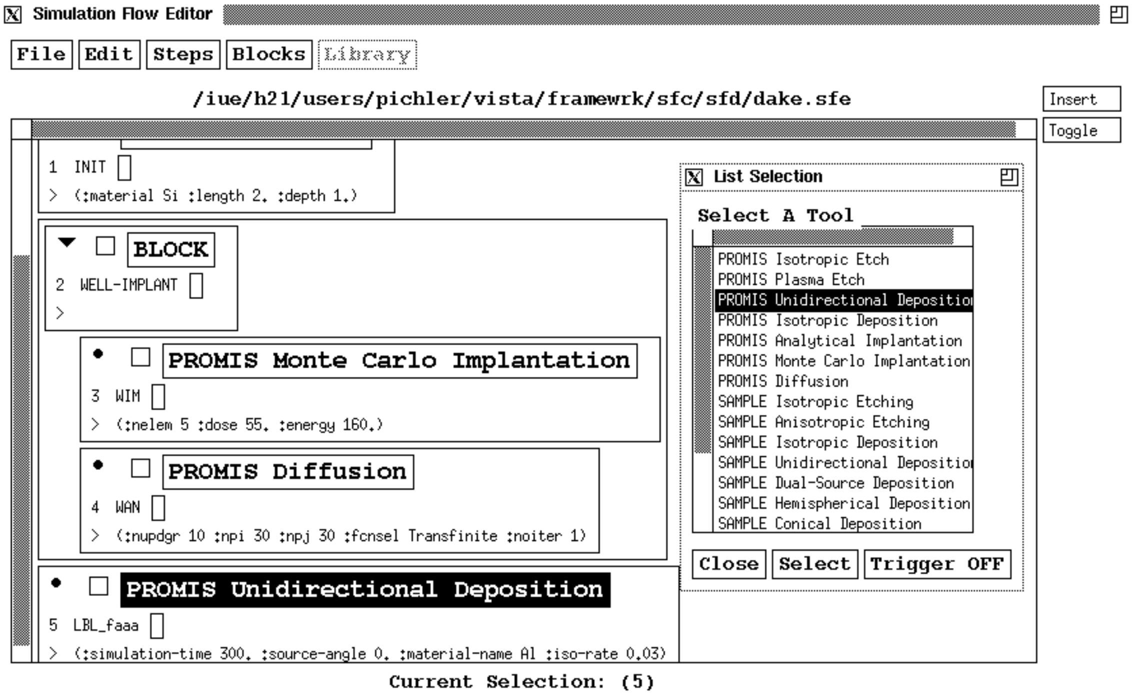

```
/iue/h21/users/pichler/vista/framewrk/sfc/sfd/dake.sfe

1  INIT □
>  (:material Si :length 2. :depth 1.)

▼ □ BLOCK
2  WELL-IMPLANT □
>

    ● □ PROMIS Monte Carlo Implantation
    3  WIM □
    >  (:nelem 5 :dose 55. :energy 160.)

    ● □ PROMIS Diffusion
    4  WAN □
    >  (:nupdgr 10 :npi 30 :npj 30 :fcnsel Transfinite :noiter 1)

● □ PROMIS Unidirectional Deposition
5  LBL_faaa □
>  (:simulation-time 300. :source-angle 0. :material-name Al :iso-rate 0.03)

Select A Tool
PROMIS Isotropic Etch
PROMIS Plasma Etch
PROMIS Unidirectional Depositio
PROMIS Isotropic Deposition
PROMIS Analytical Implantation
PROMIS Monte Carlo Implantation
PROMIS Diffusion
SAMPLE Isotropic Etching
SAMPLE Anisotropic Etching
SAMPLE Isotropic Deposition
SAMPLE Unidirectional Depositio
SAMPLE Dual-Source Deposition
SAMPLE Hemispherical Deposition
SAMPLE Conical Deposition

Current Selection: (5)
```

Figure 13: The Simulation Flow Editor

References

[1] F.P. Preparata and M.I. Shamos. *Computational Geometry.* Springer, 1985.

[2] H. Samet. *The Design and Analysis of Spatial Data Structures.* Addison Wesley, 1990.

[3] C.R. Giardina and E.R. Dougherty. *Morphological Methods in Image and Signal Processing.* Prentice-Hall, New Jersey, 1988.

[4] E. Strasser, K. Wimmer, and S. Selberherr. A New Method for Simulation of Etching and Deposition Processes. In *VPAD 93*, pp 54–55, 1993.

[5] W. Jüngling, P. Pichler, S. Selberherr, E. Guerrero, and H.W. Pötzl. Simulation of Critical IC Fabrication Processes Using Advanced Physical and Numerical Methods. *IEEE J.Solid-State Circuits*, SC-20(1):76–87, 1985.

[6] P. Pichler, W. Jüngling, S. Selberherr, E. Guerrero, and H.W. Pötzl. Simulation of Critical IC-Fabrication Steps. *IEEE Trans.Electron Devices*, ED-32(10):1940–1953, 1985.

[7] G. Hobler, E. Langer, and S. Selberherr. Two-Dimensional Modeling of Ion Implantation with Spatial Moments. *Solid-State Electron.*, 30(4):445–455, 1987.

[8] G. Hobler and S.Selberherr. Monte Carlo Simulation of Ion Implantation into Two- and Three-Dimensional Structures. *IEEE Trans.Computer-Aided Design*, CAD-8(5):450–459, 1989.

[9] H. Ryssel, J. Lorenz, and K. Hoffmann. Models for Implantation into Multilayer Targets. *Applied Physics A*, 41:201–207, 1986.

[10] R.J. Wierzbicki, J. Lorenz, and A. Barthel. Simulation of Ion Implantation into Multilayer Structures. In *ESSDERC 89*, pp 193–197, 1989.

[11] J.F. Gibbons, W.S. Johnson, and S.W. Mylroie. *Projected Range Statistics.* Halstead Press, Strandsberg, 1975.

[12] M. Simard-Normadin and C. Slaby. Empirical Modeling of Low Energy Implants in Silicon. *J.Electrochem.Soc.*, 132(9):2218–2223, 1985.

[13] G. Hobler. *Simulation der Ionenimplantation in ein-, zwei- und dreidimensionalen Strukturen.* PhD thesis, Technische Universität Wien, Austria, 1988.

[14] Ch. Pichler and S. Selberherr. Process Flow Representation within the VISTA Framework. In S. Selberherr, H. Stippel, and E. Strasser, editors, *Simulation of Semiconductor Devices and Processes*, volume 5, pp 25–28. Springer, 1993.